Journal of Hazardous Materials 467 (2024) 133755

Contents lists available at ScienceDirect

Journal of Hazardous Materials

journal homepage: www.elsevier.com/locate/jhazmat

Research Paper

Integrating molecular imprinting into flexible covalent organic frameworks for selective recognition and efficient extraction of aflatoxins

Li-Hong Su [a,b,c], Hai-Long Qian [a,b,c,d], Cheng Yang [a,b,c], Chuanxi Wang [e], Zhenyu Wang [e], Xiu-Ping Yan [a,b,c,d,*]

[a] State Key Laboratory of Food Science and Resources, Jiangnan University, Wuxi 214122, China
[b] International Joint Laboratory on Food Safety, Jiangnan University, Wuxi 214122, China
[c] Institute of Analytical Food Safety, School of Food Science and Technology, Jiangnan University, Wuxi 214122, China
[d] Key Laboratory of Synthetic and Biological Colloids, Ministry of Education, Jiangnan University, Wuxi 214122, China
[e] Institute of Environmental Processes and Pollution control, and School of Environment and Civil Engineering, Jiangnan University, Wuxi 214122, China

HIGHLIGHTS

- A novel molecular imprinted flexible covalent organic framework (MI-FCOF) is prepared.
- Flexible units endow COF with adaptability to form the imprinted cavity.
- MI-FCOF exhibits excellent selectivity for aflatoxins efficient extraction.
- MI-FCOF gives matrix-free determination of aflatoxins in real samples.

GRAPHICAL ABSTRACT

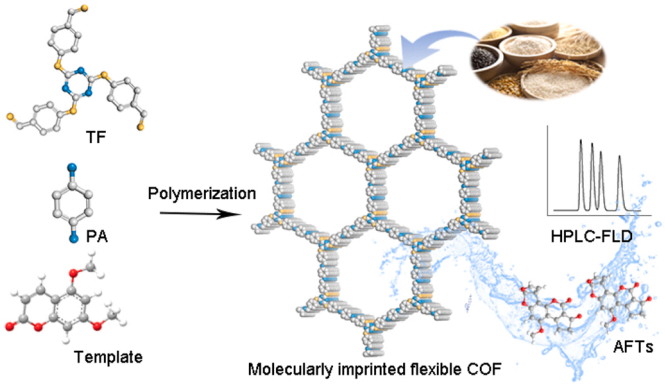

ARTICLE INFO

Keywords:
Flexible covalent organic frameworks
Molecularly imprinted polymers
Aflatoxins
Selective extraction

ABSTRACT

Covalent organic frameworks (COFs) are promising adsorbents for extraction, but their selectivity for molecular recognition remains a challenging issue due to the very limited structural design with rigid structure. Herein, we report an elegant strategy for the design and synthesis of molecularly imprinted flexible COFs (MI-FCOFs) via one-pot reaction between the flexible building block of 2,4,6-tris(4-formylphenoxy)– 1,3,5-triazine and linear 4-phenylenediamine for selective extraction of aflatoxins. The flexible chain structure enabled the developed MI-FCOF to adjust the shape and conformation of frameworks to suit the template molecule, giving high selectivity for aflatoxins recognition. Moreover, MI-FCOF with abundant imprinted sites and function groups exhibited an exceptional adsorption capacity of 258.4 mg g^{-1} for dummy template which is 3 times that of no-imprinted FCOF (NI-FCOF). Coupling MI-FCOF based solid-phase extraction with high-performance liquid chromatography gave low detection limits of 0.003–0.09 ng mL^{-1} and good precision with relative standard deviations $\leq$ 6.7% for the determination of aflatoxins. Recoveries for the spiked rice, corn, wheat and peanut samples were in the range of

* Corresponding author at: State Key Laboratory of Food Science and Resources, Jiangnan University, Wuxi 214122, China.
E-mail address: xpyan@jiangnan.edu.cn (X.-P. Yan).

https://doi.org/10.1016/j.jhazmat.2024.133755
Received 9 December 2023; Received in revised form 31 January 2024; Accepted 6 February 2024
Available online 8 February 2024

85.4%– 105.4%. The high selectivity of the developed MI-FCOF allows matrix-free determination of AFTs in food samples. This work offers a new way to the design of MI-FCOF for selective molecular recognition.

1. Introduction

Aflatoxins (AFTs), a class of secondary metabolites produced by *Aspergillus flavus* and *Aspergillus parasiticus* under natural conditions, seriously contaminate corn, rice, wheat and other food crops [16,20]. The difuran ring and coumarin structure make AFTs highly toxic at low levels to humans and animals [24,27]. Most countries have established strict limits of AFTs, such as European Union set the maximum contamination of AFB1 at 2 μg kg^{-1} in rice and peanut food, 4 μg kg^{-1} for the total amount of AFB1, AFG1, AFG2 and AFB2 [11,36,39]. Therefore, various analytical methods have been developed for the determination of AFTs, such as liquid chromatography, immunoassay and biosensing [13,49,5]. However, due to the complex sample matrix and low concentration of AFTs, a sample pretreatment step is crucial to improve the accuracy of analytical methods. Currently, solid-phase extraction (SPE) based on antibody is the most widely used for selective purification and enrichment of AFTs in sample preparation [14,22,35]. Nevertheless, it still has unavoidable problems including the complex preparation process, high cost and low stability.

Molecularly imprinted polymers (MIPs) are artificial antibodies with specific recognition sites to template molecules in size, shape and functional groups [29,40]. Owing to their good stability and potential reusability, MIPs own benefits over antibody as excellent SPE adsorbents in the field of sample pretreatment [3,30,9]. MIPs are mainly fabricated via bulk polymerization on the basis of the co-polymerization of functional monomer, cross-linker and template molecule [31,32]. However, such MIPs still suffer from several disadvantages such as complex synthesis process, deeply embedded templates, slow mass transfer and low adsorption capacity. Moreover, the limited functional monomers and cross-linking agents also hinder the further development of MIPs.

Covalent organic frameworks (COFs) are a promising type of crystalline organic porous polymers constructed from organic building blocks via covalent bonds [7]. The high specific surface area and open channel structure endow numerous accessible sites and rapid diffusion for analytes [23,46]. In addition, the predesigned structure and tunable functionality of COFs constructed from different building blocks are favorable for ion conduction, absorption and separation [28,33,44]. Very recently, these unique properties of COFs provide new possibilities to promote the development of molecularly imprinted COF (MI-COF) [25,41,45]. For instance, a magnetic MI-COF was synthesized via Schiff base reaction with 3,5-triformylphoroglucinol (Tp) as cross-linker and different building blocks as functional monomers for efficient adsorption of cyanidin-3-O-glucoside [10]. In addition, an imine-linked MI-COF was fabricated with 1,3,5-tris(4-aminophenyl)benzene and Tp as functional monomers for high selective recognition of cyano pyrethroids in plant samples [47]. However, these studies on MI-COFs mainly rely on rigid building blocks, which may not sufficiently take the advantage of the active sites and functional groups in MI-COFs. Also, the rigid linkages further restrict the adjustment of the imprinting cavities in size and shape, leading to low selectivity.

Flexible COFs (FCOFs) which contain flexible chain segments have attracted increasing attention owing to the strong spatial freedom in rotation and distortion [12,18]. Unlike rigid COFs, FCOFs feature self-adaptive capability to interact with guest molecules, creating various possibilities for structural transition during COF formation [17]. This feature of FCOFs allows dynamic 3D COFs to undergo different structural transformations with the adsorption of gas and vapors [34]. Therefore, the incorporation of flexible chain segments into porous frameworks is expected to be a promising way to fabricate molecularly imprinted FCOFs (MI-FCOFs) for molecular recognition.

Herein, we report an elegant strategy to integrate molecular imprinting into FCOFs by tuning linkers and linkages for the selective extraction of AFTs in food samples. The MI-FCOF was fabricated via one-pot reaction between 1,4-phenylenediamine (PA), 2,4,6-tris(4-formylphenoxy)– 1,3,5-triazine (TF) and template molecules. TF was chosen as the flexible building block due to the presence of C–O single bonds in the backbone with large conformational and rotational freedom. PA was used as the functional monomer to form strongly hydrophobic microenvironment for the adsorption of AFTs. In addition, formic acid (FA) was employed as the catalyst to produce C-N flexible linker unit, giving rise to adaptability to guest molecules. After the removal of template molecules, the imprinting cavities were produced with complementary to the target molecules in terms of shape and recognition sites for the specific recognition of template molecules.

2. Experimental section

2.1. Chemicals

TF, 2,6-anthracenediamine (DA), 3,3-dihydroxybenzidine (DHBD) and 1,3,5-tris-(4-aminophenyl)triazine (TZ) came from Chemsoon Co., Ltd (Shanghai, China). PA, 2,5-dimethyl-1,4-phenylenediamine (PA-2), benzidine (BD), 5,7-dimethoxycoumarin (DMC), 7-acetoxy-4-methylcoumarin (AM) and 7-ethoxycoumarin (EM) were from Shanghai Aladdin Biochemical Technology Co., Ltd (Shanghai, China). The standard solutions of AFB1, AFB2, AFG1, AFG2, zearalenone (ZEN), deoxynivalenol (DON) and ochratoxins A (OTA) were given by Anpel Laboratory Technologies Co., Ltd (Shanghai, China). Mesitylene, 1,4-dioxane, o-dichlorobenzene (o-DCB), n-butyl alcohol (n-BuOH), dimethylacetamide (DMAC), ethanol (EtOH), formic acid (FA), acetic acid (HAc), methanol (MeOH) and tetrahydrofuran (THF) were acquired from Sinopharm Chemical Reagent Co., Ltd (Shanghai, China). Ultrapure water came from Wahaha Foods Co., Ltd (Shanghai, China).

2.2. Apparatus

Powder X-ray diffraction (PXRD) measurements were performed on a D2 PHASER0 instrument with Cu Kα radiation (Bruker, Germany). Scanning electron microscopy (SEM) images were acquired on SU8100 SEM (Hitachi, Japan). Fourier transform infrared (FT-IR) spectra were collected on Nicolet 6700 spectrometer (Thermo, USA). UV–vis absorption spectra were measured on a UV-3600 PLUS spectrophotometer (Shimadzu, Japan). N_2 adsorption-desorption measurement was performed on Autosorb-IQ at 77 K (Quantachrome, USA). X-ray photoelectron spectroscopy (XPS) experiments were conducted on Thermo Kalpha (Thermo, USA).

Four AFTs were separated on a C18 column (4.6 mm × 250 mm, 5 μm) (Agilent, USA) with an e2695 HPLC (Waters, USA) equipped with a 2475 fluorescence detector (FLD) at the mobile phase (H_2O/ACN, 45:55 v/v) flow rate of 1 mL min^{-1}. Other conditions: column temperature, 35 °C; injected sample volume, 10 μL; FLD excitation wavelength, 365 nm; emission wavelength, 440 nm.

2.3. Preparation of MI-FCOF and NI-FCOF

The preparation of the MI-FCOF and NI-FCOF from TF and PA were described as follows: TF (22.1 mg, 0.05 mmol), PA (8.3 mg, 0.075 mmol) and DMC (15 mg) were mixed with 0.5 mL mesitylene/1,4-dioxane (1:1 v/v), and sonicated for 5 min. Afterwards, the aqueous solution of formic acid (0.05 mL, 6 M) was slowly added. After 20 min sonication, the mixture was degassed with three freeze–pump–thaw cycles, and then reacted at 80 ℃ for 24 h. The resulting MI-FCOF was collected by

filtration, washed with tetrahydrofuran, and eluted with MeOH:HAc (v/v, 9:1) to remove the template until no UV–vis absorbance of DMC at 327 nm was observed. Finally, the MI-FCOF was eluted with MeOH and dried at 60 ℃ under vacuum overnight. The NI-FCOF was prepared by the same process in the absence of DMC. The synthesis of other MI-FCOF and NI-FCOF based on PA-2, BD, DHBD, DA and TZ were described in Supplementary Information.

2.4. Adsorption experiments

To determine the adsorption capacity, MI-FCOF or NI-FCOF (1 mg) was dispersed in DMC (4 mL, pH 6.0) solutions with different initial concentrations (10–250 mg L^{-1}) and shaken for 1 h at room temperature. To study the adsorption kinetics, MI-FCOF or NI-FCOF (1 mg) was added to DMC solution (30 mg L^{-1}, 4 mL, pH 6.0) with different shake times (0–90 min). Then, the supernatant was collected through a 0.22 μm filter membrane for UV–vis absorption measurements. More detailed procedures are described in Supplementary Information.

2.5. Calculation of imprinting factor

Imprinting factor (IF) was calculated as the ratio of the adsorption capacity of MI-FCOF to that of NI-FCOF to evaluate imprinting efficiency.

2.6. Extraction of AFTs in real samples

Rice, corn, wheat and peanut samples were collected from the local supermarkets (Wuxi, China) and crushed with wall breaker. The samples (5 g) were thoroughly extracted with 20 mL of ACN/water solution (8:2, v/v) under ultrasonication for 30 min. Then, the supernatant was collected via centrifugation at 10000 rpm for 10 min and concentrated by a nitrogen stream. The residue was redissolved with 0.5 mL of ACN and the solution was made to 8 mL with ultrapure water for subsequent extraction. A centrifuge tube (10 mL) was charged with 2 mg of MI-FCOF and 8 mL of sample solution, and shaken at room temperature for 2 min. The MI-FCOF was separated from the solution via centrifugation at 10000 rpm and the adsorbed AFTs on MI-FCOF were eluted with 1 mL of ACN for 5 min. Finally, the eluent solution was collected through a 0.22 μm filter membrane for HPLC-FLD analysis.

2.7. Reusability test

The reusability of the MI-FCOF was tested using 5 ng mL^{-1} AFTs solution with the solid-liquid ratio of 0.25 mg mL^{-1} at pH 6.0. After one run of extraction and elution, the MI-FCOF was washed with ACN several times and dried under vacuum. The resultant material was used for another extraction experiment. The regenerated MI-FCOF was recycled six times under the same conditions to evaluate the reusability of MI-FCOF. PXRD analysis was carried out to check the stability of the MI-FCOF after regeneration.

3. Results and discussion

3.1. Design and synthesis of MI-FCOF

Rigid building block and linker mode are generally used to construct COFs to acquire ordered periodic structure and high crystallinity [8]. However, it is quite limited for the selectivity of the resulting rigid COFs to recognize guest molecules mainly based on the difference of functional groups or size exclusion mechanism. The elasticity and self-adaptability of flexible chain segments enable FCOFs to tune the pore shape and cavity environment by the entry of guest molecules. Thus, we integrated flexible building block and flexible linker into the design of MI-FCOF (Fig. 1). The flexible building block TF was selected as a cross-linker as it contains triazine ring backbone and flexible C-O single bonds. Moreover, the formation of C-N flexible linker unit after polymerization gave the FCOF more flexibility. Further change of the topology and functional monomer enabled the synthesis of MI-FCOFs with adjustable imprinted cavities and binding ability with target molecules.

MI-FCOF was synthesized through an aldehyde–amine polycondensation reaction. Note that FA was used to replace typical HAc as the catalyst due to FA can reduce the rigid C═N bond into flexible C-N linker [42]. HAc catalysis gave the prepared MI-COFs a strong FT-IR peak at 1621 cm^{-1} for the stretching vibration of C═N (Fig. S1). In

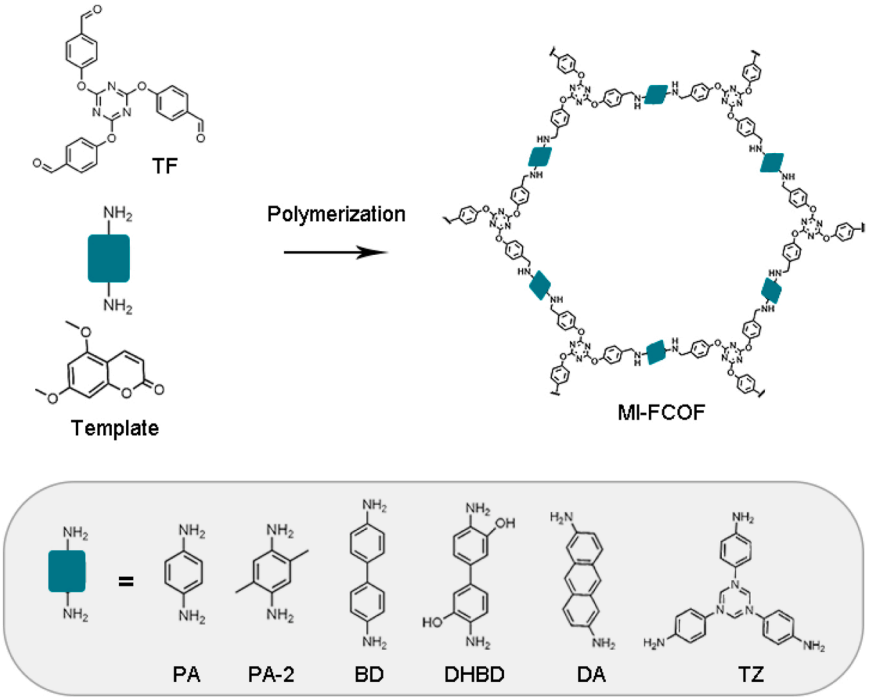

Fig. 1. Schematic diagram for the synthesis of MI-FCOF.

contrast, FA catalysis rendered the prepared MI-FCOF a strong C-N vibration peak at 1252 cm^{-1}, but weak C═N vibration peak at 1621 cm^{-1}. The self-adaptive adjustment of the flexible structure in MI-FCOF prepared with FA as catalyst gave much better imprinting efficiency for the binding with template molecules than the rigid MI-COF prepared with HAc as catalyst (Fig. S2). Thus, FA was used as catalyst for further study.

We then examined three analogues of AFTs, including DMC, AM and EM as the dummy templates to prepare MI-FCOF (Fig. S3). Dummy template can effectively avoid the occurrence of false positive results [1] as well as the use of highly toxic and expensive AFT templates. For a model analyte AFB1, DMC as the dummy template gave the prepared MI-FCOF higher adsorption capacity than AM and EM (Fig. 2A). Therefore, we selected DMC as dummy template to prepare MI-FCOF.

We also optimized the topology and the amount of functional group, solvent, and the amount of DMC for the preparation of MI-FCOFs. Functional monomers not only interact with template molecules, but also can be polymerized with cross-linker to form polymer network structure. Therefore, a series of MI-FCOFs were first prepared by varying functional groups and topological structures. The functional monomers of BD and DA gave amorphous MI-FCOFs with low IF values and adsorption capacity for DMC (Fig. 2B and S4). Obviously, PA gave the better imprinting effect with high IF value. Meanwhile, the IF value reached the maximum when the amount of PA was 0.075 mmol, so 0.075 mmol of PA was selected as the optimal amount (Fig. 2C). In addition, solvent has an important influence on imprinting process as it can adjust the solubility of building blocks and reaction rate. We found that the mixture of dioxane and mesitylene as the solvent gave better imprinting effect (Fig. 2D). In addition, when the amount of DMC increased to 15 mg, the absorption capacity of MI-COF obviously increased due to a growing number of imprinting sites (Fig. 2E). Meanwhile, the PXRD peak of (100) displayed a clear shift when the amount of DMC reached 15 mg (Fig. S5), indicating the guest-induced stretching of flexible structure. Thus, 15 mg of DMC was chosen to prepare MI-FCOF. Moreover, the largest IF value was obtained when the polymerization time was 24 h (Fig. 2F).

3.2. Characterization of MI-FCOFs and NI-FCOFs

The prepared NI-FCOFs and MI-FCOFs were characterized by PXRD, N_2 adsorption and SEM experiments. We systematically analyzed the crystalline structure of MI-FCOF and NI-FCOF by combining experimental PXRD with possible simulated structures. The MI-FCOF gave the PXRD peaks of (100), (110), (200) and (210) facets at $2\theta = 2.61°$, 4.68°, 5.34° and 7.21°, respectively (Fig. 3A). The MI-FCOF adopted an AA stacking mode in a P6/M space group with the unit cell parameters of a = b= 39.66 Å, c = 3.51 Å, $\alpha = \beta = 90°$, $\gamma = 120°$, and the corresponding R_{wp} of 4.86% and R_p of 3.82%. The crystalline structure of the NI-FCOF was also consistent well with the that of AA-stacking mode (space group: P6/M; unit cell parameters: a = b=37.33 Å, c =3.51 Å, $\alpha = \beta = 90°$, $\gamma = 120°$, the corresponding R_{wp} of 4.43% and R_p of 3.55%) (Fig. 3B). However, the NI-FCOF showed an obvious shift of the (100) facet toward a larger angle $2\theta = 2.72°$ in comparison with the MI-FCOF at $2\theta = 2.61°$ (Fig. 3C). In addition, the MI-FCOF gave larger in-plane unit cell parameters of 2.33 Å at a and b than the NI-FCOF. This phenomenon may be attributed to the shrinkage of the flexible structure of the NI-FCOF without template molecules, leading to a small pore size.

The porous structures of the MI-FCOF and NI-FCOF were further investigated by N_2 adsorption-desorption experiments. The MI-FCOF and NI-FCOF offered Brunauer–Emmett–Teller (BET) surface areas of 1259 and 1100 $m^2\ g^{-1}$, respectively (Fig. 3D). In addition, the N_2 adsorption-desorption isotherms of MI-FCOF and NI-FCOF displayed hysteresis on desorption, indicating the presence of the flexible framework of MI-FCOF and NI-FCOF [43,48]. The pore size distributions of MI-FCOF and NI-FCOF based on nonlocal density functional theory (NLDFT) were centered at around 3.3 and 2.1 nm, respectively (Fig. S6). Compared with the NI-FCOF, the MI-FCOF gave a relatively larger BET surface area and pore size due to the twisting and stretching of the chain segment in space with the introduction of template molecules. Moreover, the SEM images show the uniform spheres-like morphology for the NI-FCOF and MI-FCOF (Figs. 3E and 3F). The MI-FCOF still kept its crystal structure after soaking in different solvents including 0.1 M HCl, MeOH, HAc and THF for 24 h, indicating the good stability of the MI-FCOF (Fig. S7).

3.3. Adsorption performance of MI-FCOF

We take the dummy template DMC as a model to reveal the adsorption performance of MI-FCOF for AFTs owing to the high toxicity

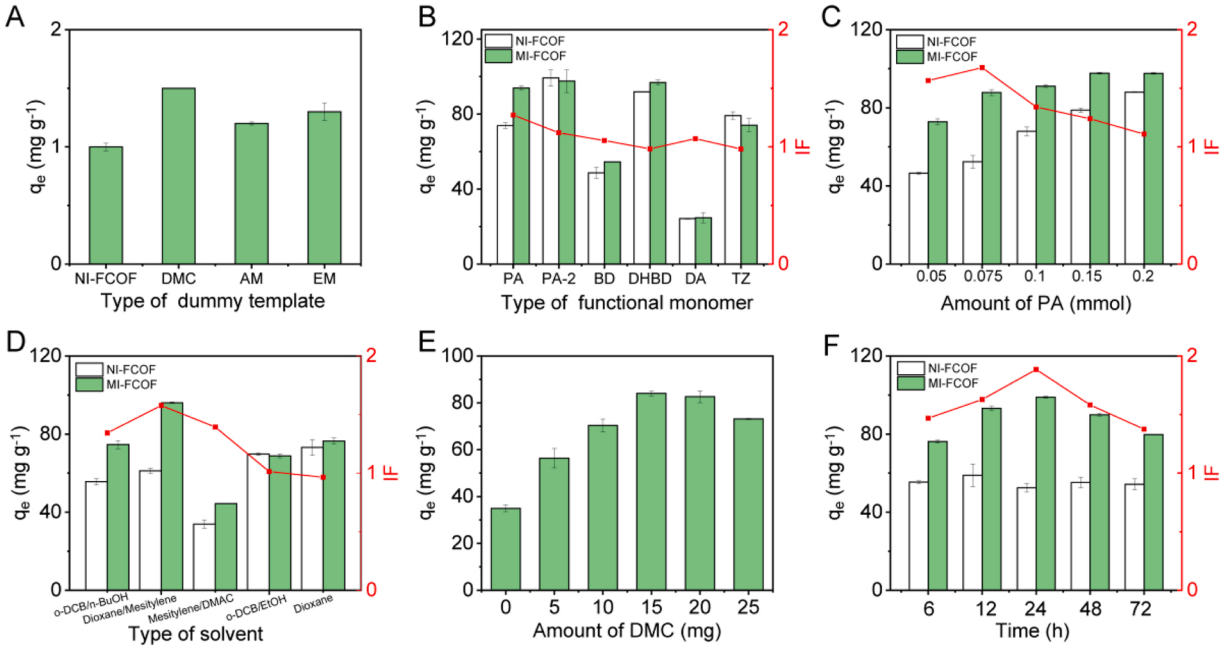

Fig. 2. Effects on the adsorption capacity and the IF value of the prepared MI-FCOF: (A) dummy template; (B) functional monomer; (C) amount of PA; (D) type of solvent; (E) amount of DMC; (F) polymerization time. Other conditions: 4 mL of 30 mg L^{-1} DMC solution at pH 6.0; 1 mg MI-FCOF or NI-FCOF.

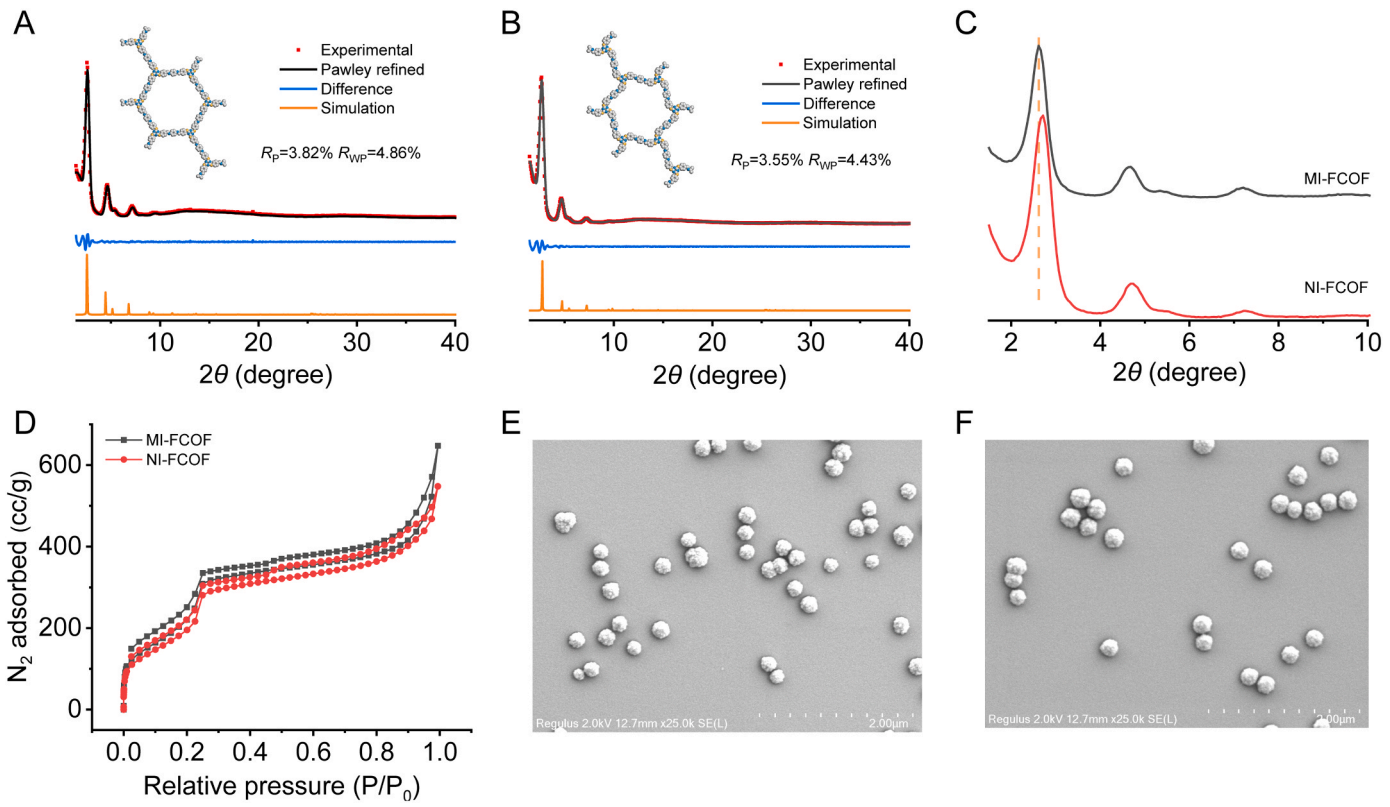

Fig. 3. Experimental, pawley refined and simulated (AA stacking model) PXRD patterns: (A) MI-FCOF; (B) NI-FCOF. (C) Comparison of the PXRD patterns of MI-FCOF and NI-FCOF. (D) N_2 sorption isotherms of MI-FCOF and NI-FCOF. SEM images: (E) NI-FCOF; (F) MI-FCOF.

of AFTs. The adsorption kinetics was tested with 1 mg MI-FCOF or NI-FCOF in the solution of 30 mg L^{-1} DMC (4 mL, pH 6.0). Obviously, the adsorption on MI-FCOF reached equilibrium within 3 min (Fig. 4 A), suggesting a fast adsorption due to the large surface area and imprinted sites of the MI-FCOF. In contrast, a much longer time of 20 min was needed to reach adsorption equilibrium for NI-FCOF. The adsorption kinetics of MI-FCOF and NI-FCOF was fitted well with the pseudo-second-order model, with R^2 of 1 and 0.9995, respectively (Fig. 4B and S8A, Table S1) [37].

The adsorption isotherms of MI-FCOF and NI-FCOF were evaluated with different initial concentrations of DMC. The adsorption capacity of MI-FCOF increased rapidly with the initial concentration of DMC from 10 to 120 mg L^{-1}, while that of the NI-FCOF changed slowly and reached equilibrium at 50 mg mL^{-1} (Fig. 4 C). The adsorption of MI-FCOF was fitted better to the Langmuir model (Fig. 4D and S8B, Table S2). Furthermore, the maximum adsorption capacity of DMC on MI-FCOF calculated by the Langmuir model was 258.4 mg g^{-1}, which was 3 times that of NI-FCOF (86.8 mg g^{-1}).

Adsorption selectivity was further tested to evaluate the performance of MI-FCOF. MI-FCOF exhibited larger adsorption capacity toward AFTs than other mycotoxins (Fig. 4 F). The low adsorption capacities for ZEN, DON and OTA resulted from the different chemical structures of these three mycotoxins and DMC template molecule (Figs. S3 and 4E). The selectivity factor was defined as the ratio of the adsorption capacity of AFB1 to other mycotoxins. The selectivity factors for AFB1 toward ZEN, DON and OTA were 2.2, 3.6 and 9.2, respectively. The binding energies calculated based on Material Studio software show that MI-FCOF gave the strongest interaction with AFTs (Fig. S9), agreeing with the experimental results. The abovementioned results indicate that the developed MI-FCOF gave high selectivity for the recognition of AFTs.

3.4. Adsorption mechanism

The developed MI-FCOF possessed abundant imprinted sites, functional groups and high hydrophobicity for favorable adsorption of AFTs. The introduced flexible units into MI-FCOF generated the imprinted cavity for the selective recognition of AFTs. Meanwhile, the abundant benzene rings, hydrogen bond donor and acceptor in the MI-FCOF gave potential π–π, hydrophobic and hydrogen bond interactions with AFTs. In addition, the high surface area and larger pore size of the MI-FCOF were conducive to the diffusion and adsorption of target analysts. Taking AFB1 as a model analyte, we utilized FT-IR and XPS to study the interactions between AFTs and MI-FCOF. After the adsorption of AFB1, the FT-IR peak for aromatic ring stretching shifted from 1567.3 and 1504.5 cm^{-1} to 1565.3 and 1503 cm^{-1}, respectively (Fig. S10), indicating the hydrophobic reaction and π − π interaction between MI-FCOF and AFB1 [16,38]. Meanwhile, the characteristic XPS peaks of C 1 s for C-C/C═C and C-N slightly shifted from 283.9 and 258.1 eV to 283.7 and 284.9 eV (Fig. S11), respectively, due to the π − π interaction in the adsorption process [15,2,21]. Moreover, the XPS peak of N 1 s at 399.5, 398.6 and 397.9 eV shifted to 399.1, 398.4 and 397.8 eV, respectively (Fig. S12), due to the hydrogen bonding between MI-FCOF and AFB1 [4, 6].

3.5. Optimization of extraction conditions

The potential parameters for SPE, such as extraction time, amount of MI-FCOF, sample pH, desorption solvent, eluent volume and eluent time were optimized with 5 ng mL^{-1} AFTs. The peak area of AFTs increased with the amount of MI-FCOF up to 2 mg, then levelled off with a further increase of the amount of MI-FCOF (Fig. 5A). Hence, 2 mg of MI-FCOF was used in subsequent experiments. In addition, the peak area of AFTs exhibited no significant change in an extraction time range of 2–20 min (Fig. 5B), so 2 min was used as extraction time. With the

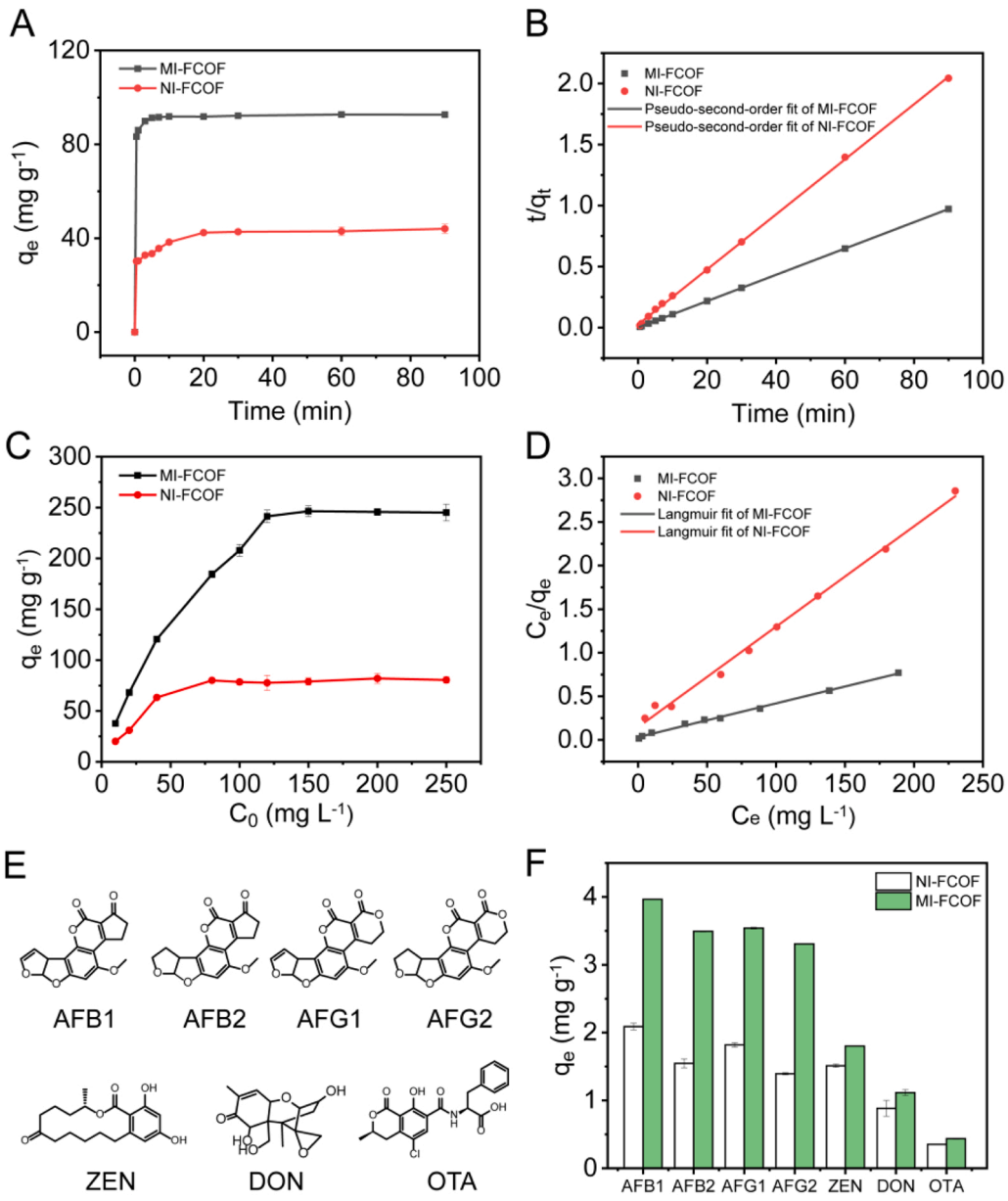

Fig. 4. (A) Adsorption kinetics of MI-FCOF and NI-FCOF (1 mg) for the adsorption of 30 mg L^{-1} DMC (4 mL, pH 6.0). (B) Pseudo-second-order isotherms of MI-FCOF and NI-FCOF. (C) Adsorption isotherms of MI-FCOF and NI-FCOF (1 mg) for 10–250 mg L^{-1} DMC solutions (4 mL, pH 6.0). (D) Langmuir isotherm of MI-FCOF and NI-FCOF. (E) Chemical structure of AFB1, AFB2, AFG1, AFG2, ZEN, DON and OTA. (F) Adsorption selectivity of MI-FCOF and NI-FCOF (1 mg) for the adsorption of 1 mg L^{-1} mycotoxins (4 mL, pH 6.0). All experiments were performed at room temperature.

increase of pH from 3 to 7, the peak area of AFTs did not show obvious change (Fig. 5C). As pH further increased, the peak area of AFTs decreased due to the decomposition of the ester ring of AFTs under alkaline condition [16]. Among the studied solvents for desorption, 1 mL of ACN gave the best elution efficiency toward AFTs (Figs. 5D and 5E). The peak area gradually increased with the increase of eluent time up to 5 min, then levelled off (Fig. 5F), so 5 min was used to ensure the complete elution of AFTs.

3.6. Validation of analytical method

The analytical performance of the developed MI-FCOF based SPE in combination with HPLC-FLD for the determination of AFTs was evaluated by testing the standard solution of AFTs. The developed method showed a wide linear range from 0.01 (AFB2) or 0.02 (AFG2) or 0.2 (AFB1) or 0.3 (AFG1) to 200 ng mL^{-1} with the determination coefficient (R^2) $\geq$ 0.9995 (Table 1). The limits of quantification (LOQs, $S/N = 10$) and limits of detection (LODs, $S/N = 3$) were in the range of 0.01 (AFB2)–0.3 ng mL^{-1} (AFG1) and 0.003 (AFB2)–0.09 ng mL^{-1} (AFG1), respectively. The relative standard deviations (RSDs, n = 6) for the determination of 5 ng mL^{-1} AFTs were 1.5–3.9% (intraday) and 2.9–6.7% (interday). Six repeated extraction-elution cycles on MI-FCOF led to no obvious change in the peak area of AFTs (Fig. S13A) as well as the crystalline structure of MI-FCOF (Fig. S13B), indicating the good reusability for the developed MI-FCOF based SPE method. Competitive extraction experiments were performed with AFTs and three other competing mycotoxins. The extraction efficiency of MI-FCOF and MI-COF for AFTs was $\geq$ 90.1% and $\geq$ 70.1%, respectively (Fig. S14), indicating the high selectivity and anti-interference ability of MI-FCOF. Compared with previous methods based on other adsorbents, the developed MI-FCOF based SPE method gave lower LODs and wider detection range (Table S3).

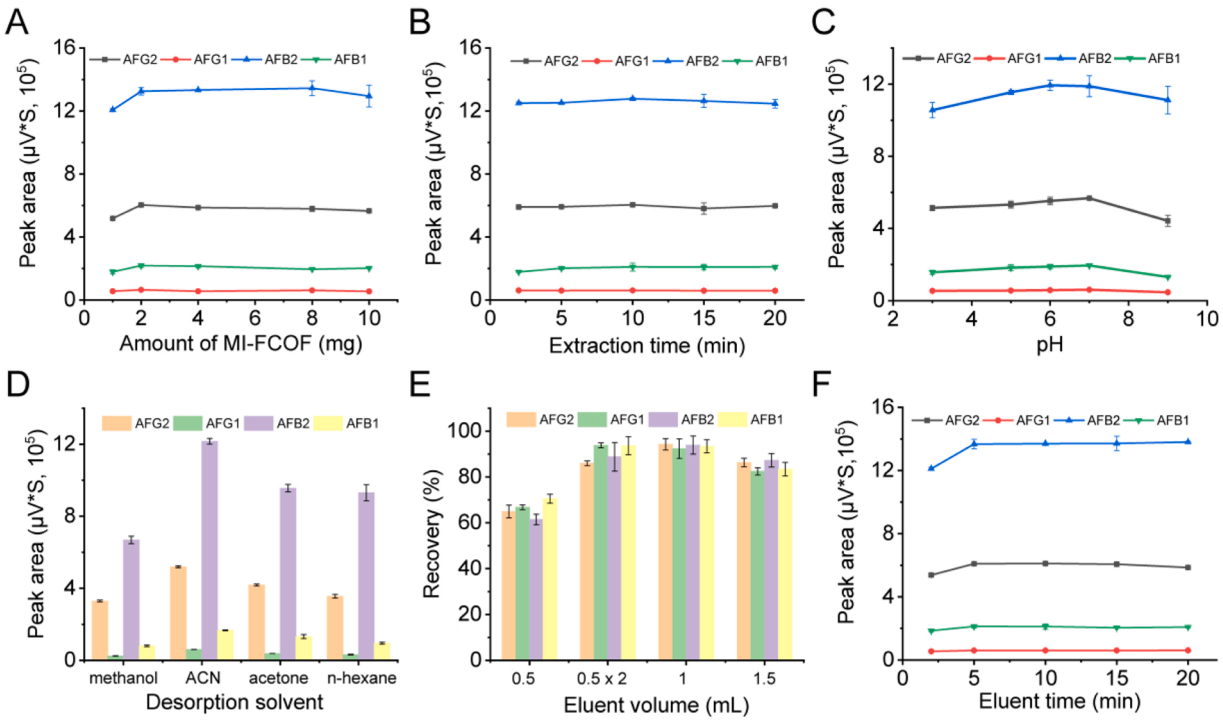

Fig. 5. Optimization of extraction conditions: (A) amount of MI-FCOF (AFTs concentration, 5 ng mL^{-1} at pH 6.0; extraction time, 2 min); (B) extraction time (amount of MI-FCOF, 2 mg; AFTs concentration, 5 ng mL^{-1} at pH 6.0); (C) sample pH (amount of MI-FCOF, 2 mg; AFTs concentration, 5 ng mL^{-1}; extraction time: 2 min); (D) desorption solvent (eluent volume, 1 mL; eluent time, 5 min); (E) eluent volume (eluent time: 5 min); (F) eluent time (1 mL ACN). 1 mL ACN was used for 5 min elution (A-C), while 2 mg of MI-FCOF was used for the extraction of 5 ng mL^{-1} AFT solution (pH 6.0) for 2 min (D-F).

Table 1
Analytical performance of the developed SPE method based on MI-FCOF.

Analyte	Linear range (ng mL^{-1})	R^2	LODs (ng mL^{-1})	LOQs (ng mL^{-1})	RSD (%)	
					Intraday ($n = 6$)	Interday ($n = 6$)
AFG2	0.02-200	0.9996	0.006	0.02	1.5	2.9
AFG1	0.3-200	0.9999	0.09	0.3	3.4	6.7
AFB2	0.01-200	0.9996	0.003	0.01	3.6	5.2
AFB1	0.2-200	0.9995	0.06	0.2	3.9	5.8

3.7. Analysis of real samples

The developed MI-FCOF based SPE in combination with HPLC-FLD was applied to the analysis of rice, corn, wheat and peanut samples for AFTs. Calibration functions (curves) were obtained by using simple standard solution and the standard additions method to check matrix effect (ME). The value of matrix effect is determined as the ratio of sensitivity in sample matrix to that in standard solution. The ME values in the range of 0.8–1.2 are generally considered negligible matrix effect [19,26]. In this work, the ME values of MI-FCOF in rice, corn, wheat and peanut samples ranged from 0.9297 to 1.005 for AFTs (Fig. S15; Table S4-S7), indicating negligible matrix effect due to the excellent selectivity of the developed MI-FCOF. Therefore, a simple standard calibration was used for the quantification of AFTs in real samples. As shown in Table 2, only AFB2 in rice 2 and wheat 2 samples were found to be 0.027 and 0.017 μg kg^{-1}, respectively, but below the limits set by European Union. To further evaluate the accuracy of the developed method, different concentrations of AFTs (2, 5 and 10 μg kg^{-1}) were spiked into food samples. The recoveries were acceptable in the range of 85.4–105.9%, indicating that the developed method gave a good accuracy for the determination of AFTs in food samples.

4. Conclusion

In conclusion, we have reported an elegant strategy to integrate molecular imprinting into FCOFs by tuning linkers and linkages. Introducing flexible chain segment to COFs allows MI-FCOF to adapt to template molecules by regulating molecular conformation for the selective recognition of AFTs. Taking the advantage of porous channels and abundant imprinted sites, the fabricated MI-FCOF exhibited large adsorption capacity and fast adsorption kinetics. The use of the prepared MI-FCOF as SPE absorbent allows selective extraction and sensitive determination of AFTs in food samples without matrix effect. The unexpected flexibility of MI-FCOF paves a way to selective adsorption and further broadens the application of COFs as functional materials.

Environmental implication

Aflatoxins are highly toxic metabolites of Aspergillus flavus and Aspergillus parasiticus and pose seriously contaminate environment and agricultural products. Aflatoxins potentially threat human health through the food chain, such as teratogenic, nephrotoxic and carcinogenic. Development of an efficient detection method to monitor aflatoxins is very important to ensure environmental and food safety, but the complex sample matrix seriously affects the detection sensitivity and accuracy. Herein, we report an elegant strategy for the integrating molecular imprinting into flexible covalent organic frameworks to selective recognition and efficient extraction of aflatoxins, providing a promising method to matrix-free determination of aflatoxins in food samples.

CRediT authorship contribution statement

Yang Cheng: Resources, Methodology. **Wang Chuanxi:** Software, Methodology. **Wang Zhenyu:** Writing – review & editing, Conceptualization. **Yan Xiu-Ping:** Writing – review & editing, Validation, Project administration, Funding acquisition, Formal analysis,

Table 2
Analytical results (mean ± SD, $n = 5$) for the determination of AFTs in food samples.

Samples	AFTs	Found (μg kg^{-1})	2 μg kg^{-1} spiked		5 μg kg^{-1} spiked		10 μg kg^{-1} spiked	
			Found (μg kg^{-1})	Recovery (%)	Found (μg kg^{-1})	Recovery (%)	Found (μg kg^{-1})	Recovery (%)
Rice 1	AFG2	ND[a]	1.93 ± 0.01	96.7 ± 0.3	4.21 ± 0.11	86.7 ± 2.1	9.05 ± 0.69	90.5 ± 6.9
	AFG1	ND[a]	1.90 ± 0.10	95.1 ± 5.1	4.86 ± 0.24	99.2 ± 4.8	9.33 ± 0.66	93.2 ± 6.6
	AFB2	<LOQ	1.89 ± 0.01	94.5 ± 0.5	4.21 ± 0.25	89.9 ± 4.9	8.81 ± 0.89	88.1 ± 8.9
	AFB1	ND[a]	1.99 ± 0.11	99.4 ± 5.6	4.45 ± 0.22	95.5 ± 4.3	8.84 ± 0.11	88.4 ± 1.1
Rice 2	AFG2	ND[a]	1.71 ± 0.04	85.4 ± 2.1	4.28 ± 0.31	85.6 ± 6.1	8.78 ± 0.84	87.8 ± 8.4
	AFG1	ND[a]	1.73 ± 0.19	86.5 ± 9.3	4.78 ± 0.17	95.5 ± 3.3	9.63 ± 0.83	96.3 ± 8.3
	AFB2	0.027 ± 0.001	1.72 ± 0.05	85.9 ± 4.3	4.58 ± 0.36	91.4 ± 7.2	9.43 ± 0.83	94.3 ± 8.3
	AFB1	ND[a]	1.98 ± 0.07	98.9 ± 3.5	4.35 ± 0.12	86.9 ± 2.5	9.49 ± 0.57	94.9 ± 5.7
Corn 1	AFG2	ND[a]	1.95 ± 0.04	97.3 ± 1.8	4.39 ± 0.39	87.9 ± 7.7	9.04 ± 0.57	90.4 ± 5.7
	AFG1	ND[a]	2.12 ± 0.12	105.9 ± 6.1	4.78 ± 0.23	95.5 ± 4.5	9.17 ± 0.47	91.7 ± 4.7
	AFB2	ND[a]	1.79 ± 0.13	89.9 ± 6.4	5.11 ± 0.23	102.2 ± 4.6	9.04 ± 0.07	90.4 ± 0.7
	AFB1	ND[a]	1.84 ± 0.13	92.2 ± 6.4	4.75 ± 0.19	94.9 ± 3.8	8.81 ± 0.35	88.1 ± 3.5
Corn 2	AFG2	ND[a]	1.97 ± 0.01	98.6 ± 0.4	4.49 ± 0.34	89.8 ± 6.8	9.04 ± 0.57	90.4 ± 5.7
	AFG1	ND[a]	2.01 ± 0.17	100.1 ± 8.6	4.73 ± 0.21	94.6 ± 4.2	9.14 ± 0.51	91.4 ± 5.1
	AFB2	ND[a]	1.81 ± 0.13	90.7 ± 6.4	5.13 ± 0.28	102.7 ± 5.5	9.23 ± 0.35	92.3 ± 3.5
	AFB1	ND[a]	2.02 ± 0.11	101.2 ± 5.4	4.71 ± 0.32	94.1 ± 6.4	9.01 ± 0.31	90.1 ± 3.1
Wheat 1	AFG2	ND[a]	1.75 ± 0.03	87.3 ± 1.4	4.28 ± 0.39	85.5 ± 7.9	8.54 ± 0.26	85.4 ± 2.6
	AFG1	ND[a]	1.96 ± 0.05	97.9 ± 0.2	4.31 ± 0.35	86.2 ± 7.1	8.91 ± 0.14	89.1 ± 1.4
	AFB2	ND[a]	1.73 ± 0.15	86.7 ± 0.1	4.63 ± 0.45	92.6 ± 9.1	8.77 ± 0.01	87.8 ± 0.1
	AFB1	ND[a]	1.77 ± 0.17	88.3 ± 8.6	4.31 ± 0.19	86.1 ± 3.9	9.05 ± 0.16	90.5 ± 1.6
Wheat 2	AFG2	ND[a]	1.92 ± 0.03	96.1 ± 1.6	4.46 ± 0.38	89.3 ± 7.6	8.64 ± 0.56	86.4 ± 5.6
	AFG1	ND[a]	1.92 ± 0.11	95.9 ± 5.5	4.42 ± 0.45	88.4 ± 8.9	8.72 ± 0.27	87.2 ± 2.7
	AFB2	0.017 ± 0.001	1.81 ± 0.08	90.3 ± 3.9	4.79 ± 0.39	95.9 ± 7.9	8.65 ± 0.27	86.5 ± 2.7
	AFB1	ND[a]	2.03 ± 0.11	101.5 ± 5.3	4.59 ± 0.34	91.8 ± 6.7	8.55 ± 0.43	85.5 ± 4.3
Peanut 1	AFG2	ND[a]	1.73 ± 0.03	86.6 ± 1.7	4.29 ± 0.21	85.7 ± 4.2	10.05 ± 0.07	100.5 ± 0.7
	AFG1	ND[a]	1.85 ± 0.05	92.4 ± 0.2	4.33 ± 0.37	86.7 ± 7.4	9.83 ± 0.39	98.3 ± 3.9
	AFB2	ND[a]	1.78 ± 0.06	88.8 ± 2.9	4.91 ± 0.29	98.1 ± 5.8	10.13 ± 0.06	101.3 ± 0.6
	AFB1	ND[a]	1.83 ± 0.11	91.3 ± 5.2	4.57 ± 0.19	91.4 ± 3.7	10.54 ± 0.25	105.4 ± 2.5
Peanut 2	AFG2	ND[a]	1.96 ± 0.02	98.1 ± 0.9	4.03 ± 0.17	86.1 ± 3.3	9.09 ± 0.15	90.9 ± 1.5
	AFG1	ND[a]	1.73 ± 0.04	86.7 ± 1.8	4.47 ± 0.29	89.4 ± 5.9	9.43 ± 0.26	94.3 ± 2.6
	AFB2	ND[a]	1.95 ± 0.12	97.3 ± 6.2	4.91 ± 0.15	95.1 ± 2.9	9.39 ± 0.15	93.9 ± 1.5
	AFB1	ND[a]	1.79 ± 0.09	89.3 ± 4.4	4.62 ± 0.12	92.4 ± 2.4	9.91 ± 0.16	99.1 ± 1.6

ND: not detected.

Conceptualization. **Su Li-Hong:** Writing – original draft, Validation, Methodology, Investigation, Data curation, Conceptualization. **Qian Hai-Long:** Validation, Investigation.

Declaration of competing interest

The authors declare that they have no known competing financial interests or personal relationships that could have appeared to influence the work reported in this paper.

Data availability

Data will be made available on request.

Acknowledgements

We greatly appreciate the financial support from the National Natural Science Foundation of China (22176073 and 22076066), the Program of "Collaborative Innovation Center of Food Safety and Quality Control in Jiangsu Province", and the Postgraduate Research & Practice Innovation Program of Jiangsu Province (KYCX23_2512).

Appendix A. Supporting information

Supplementary data associated with this article can be found in the online version at doi:10.1016/j.jhazmat.2024.133755.

References

[1] Chen, R.N., Kang, S.H., Li, J., Lu, L.N., Luo, X.P., Wu, L., 2021. Comparison and recent progress of molecular imprinting technology and dummy template molecular imprinting technology. Anal Methods 13, 4538–4556. https://doi.org/10.1039/d1ay01014j.

[2] Cheng, J., Wang, B., Lv, J., Wang, R., Du, Q., Liu, J., Yu, L., Dong, S., Li, J.R., Wang, P., 2021. Remarkable uptake of deoxynivalenol in stable metal-organic frameworks. ACS Appl Mater Interfaces 13, 58019–58026. https://doi.org/10.1021/acsami.1c19501.

[3] Cui, Y., He, Z., Xu, Y., Su, Y., Ding, L., Li, Y., 2021. Fabrication of molecularly imprinted polymers with tunable adsorption capability based on solvent-responsive cross-linker. Chem Eng J 405, 126608. https://doi.org/10.1016/j.cej.2020.126608.

[4] Du, Z.-D., Cui, Y.-Y., Yang, C.-X., Yan, X.-P., 2019. Core–shell magnetic amino-functionalized microporous organic network nanospheres for the removal of tetrabromobisphenol a from aqueous solution. ACS Appl Nano Mater 2, 1232–1241. https://doi.org/10.1021/acsanm.8b02119.

[5] Eivazzadeh-Keihan, R., Pashazadeh, P., Hejazi, M., de la Guardia, M., Mokhtarzadeh, A., 2017. Recent advances in nanomaterial-mediated bio and immune sensors for detection of aflatoxin in food products. Trends Anal Chem 87, 112–128. https://doi.org/10.1016/j.trac.2016.12.003.

[6] Fu, D., Zhang, Q., Chen, P., Zheng, X., Hao, J., Mo, P., Liu, H., Liu, G., Lv, W., 2021. Efficient removal of bisphenol pollutants on imine-based covalent organic frameworks: adsorption behavior and mechanism. RSC Adv 11, 18308–18320. https://doi.org/10.1039/d1ra02342j.

[7] Guan, Q., Zhou, L.L., Dong, Y.B., 2023. Construction of covalent organic frameworks via multicomponent reactions. J Am Chem Soc 145, 1475–1496. https://doi.org/10.1021/jacs.2c11071.

[8] Guo, X., Tian, Y., Zhang, M., Li, Y., Wen, R., Li, X., Li, X., Xue, Y., Ma, L., Xia, C., Li, S., 2018. Mechanistic insight into hydrogen-bond-controlled crystallinity and adsorption property of covalent organic frameworks from flexible building blocks. Chem Mater 30, 2299–2308. https://doi.org/10.1021/acs.chemmater.7b05121.

[9] Hao, Y.X., Yang, M.L., Chen, X.F., Zhang, F., Li, N., He, M.Y., Xu, M.X., 2023. Development of magnetic molecularly imprinted polymer coupled nanospray ion source for analysis of cephalosporin antibiotics in food samples. J Agric Food Chem 71, 8656–8664. https://doi.org/10.1021/acs.jafc.3c01527.

[10] Ji, W., Sun, R., Geng, Y., Liu, W., Wang, X., 2018. Rapid, low temperature synthesis of molecularly imprinted covalent organic frameworks for the highly selective extraction of cyano pyrethroids from plant samples. Anal Chim Acta 1001, 179–188. https://doi.org/10.1016/j.aca.2017.12.001.

[11] Jia, M., Yu, L., Li, X., Li, Y., He, X., Chen, L., Zhang, Y., 2023. An aptamer-functionalized photonic crystal sensor for ultrasensitive and label-free detection of aflatoxin B1. Talanta 260, 124638. https://doi.org/10.1016/j.talanta.2023.124638.

[12] Kang, C., Zhang, Z., Kusaka, S., Negita, K., Usadi, A.K., Calabro, D.C., Baugh, L.S., Wang, Y., Zou, X., Huang, Z., Matsuda, R., Zhao, D., 2023. Covalent organic framework atropisomers with multiple gas-triggered structural flexibilities. Nat Mater 22, 636–643. https://doi.org/10.1038/s41563-023-01523-2.
[13] Karami-Osboo, R., Ahmadpoor, F., Nasrollahzadeh, M., Maham, M., 2022. Polydopamine-coated magnetic spirulina nanocomposite for efficient magnetic dispersive solid-phase extraction of aflatoxins in pistachio. Food Chem 377, 131967. https://doi.org/10.1016/j.foodchem.2021.131967.
[14] Kuang, J., Ju, J., Lu, Y., Chen, Y., Liu, C., Kong, D., Shen, W., Shi, H.W., Li, L., Ye, J., Tang, S., 2023. Magnetic three-phase single-drop microextraction for highly sensitive detection of aflatoxin B1 in agricultural product samples based on peroxidase-like spatial network structure. Food Chem 416, 135856. https://doi.org/10.1016/j.foodchem.2023.135856.
[15] Li, H.-Z., Yang, C., Qian, H.-L., Yan, X.-P., 2023. Room-temperature synthesis of ionic covalent organic frameworks for efficient removal of diclofenac sodium from aqueous solution. Sep Purif Technol 306, 122704. https://doi.org/10.1016/j.seppur.2022.122704.
[16] Li, J., Yang, Y., Zhou, Z., Li, S., Hao, L., Liu, W., Wang, Z., Wu, Q., Wang, C., 2023. Fluorine-functionalized triazine-based porous organic polymers for the efficient adsorption of aflatoxins. J Agric Food Chem 71, 3068–3078. https://doi.org/10.1021/acs.jafc.2c08063.
[17] Li, Y., Sui, J., Cui, L.S., Jiang, H.L., 2023. Hydrogen bonding regulated flexibility and disorder in hydrazone-linked covalent organic frameworks. J Am Chem Soc 145, 1359–1366. https://doi.org/10.1021/jacs.2c11926.
[18] Liu, X., Li, J., Gui, B., Lin, G., Fu, Q., Yin, S., Liu, X., Sun, J., Wang, C., 2021. A crystalline three-dimensional covalent organic framework with flexible building blocks. J Am Chem Soc 143, 2123–2129. https://doi.org/10.1021/jacs.0c12505.
[19] Liu, Y., Ling, Y., Zhang, Y., Feng, X., Zhang, F., 2023. Synthesis of a magnetic covalent organic framework for extraction and separation of ultraviolet filters in beverage samples. Food Chem 410, 135323. https://doi.org/10.1016/j.foodchem.2022.135323.
[20] Lu, T., Fu, C., Xiong, Y., Zeng, Z., Fan, Y., Dai, X., Huang, X., Ge, J., Li, X., 2023. Biodegradation of aflatoxin B1 in peanut oil by an amphipathic laccase-inorganic hybrid nanoflower. J Agric Food Chem 71, 3876–3884. https://doi.org/10.1021/acs.jafc.2c08148.
[21] Ma, F., Guo, Q., Zhang, Z., Ding, X., Zhang, L., Li, P., Yu, L., 2023. Simultaneous removal of aflatoxin B1 and zearalenone in vegetable oils by hierarchical fungal mycelia@graphene oxide@Fe_3O_4 adsorbent. Food Chem 428, 136779. https://doi.org/10.1016/j.foodchem.2023.136779.
[22] Ni, B., Ye, J., Chen, J., Li, L., Liu, H., Wu, Y., Wang, S., 2022. Surfactant-enhanced and automated pretreatment based on immunoaffinity magnetic beads coupled with ultra-performance liquid chromatography with fluorescence detection for the determination of aflatoxins in peanut oils. J Agric Food Chem 70, 10654–10661. https://doi.org/10.1021/acs.jafc.2c02529.
[23] Qiu, J., Xu, C., Xu, X., Zhao, Y., Zhao, Y., Zhao, Y., Wang, J., 2023. Porous covalent organic framework based hydrogen-bond nanotrap for the precise recognition and separation of gold. Angew Chem Int Ed 62, e202300459. https://doi.org/10.1002/anie.202300459.
[24] Song, C.-G., Liu, Y.-Q., Ding, G., Yang, J., Wang, C.-Y., Wu, J.-R., Wu, G., Li, M.-H., Guo, L.-P., Qin, J.-C., Yang, Y.-W., 2022. Synergistic adsorption–photocatalysis based on magnetic metal–organic framework nanoplatforms for organic pollutant removal. ACS Appl Nano Mater 5, 18930–18939. https://doi.org/10.1021/acsanm.2c04734.
[25] Su, L.H., Qian, H.L., Yang, C., Wang, C., Wang, Z., Yan, X.P., 2023. Surface imprinted-covalent organic frameworks for efficient solid-phase extraction of fluoroquinolones in food samples. J Hazard Mater 459, 132031. https://doi.org/10.1016/j.jhazmat.2023.132031.
[26] Sun, W., Xu, Q., Liu, Q., Wang, T., Liu, Z., 2023. Post-synthetic modification of a magnetic covalent organic framework with alkyne linkages for efficient magnetic solid-phase extraction and determination of trace basic orange II in food samples. J Chromatogr A 1690, 463777. https://doi.org/10.1016/j.chroma.2023.463777.
[27] Tao, F., Yao, H., Hruska, Z., Burger, L.W., Rajasekaran, K., Bhatnagar, D., 2018. Recent development of optical methods in rapid and non-destructive detection of aflatoxin and fungal contamination in agricultural products. Trends Anal Chem 100, 65–81. https://doi.org/10.1016/j.trac.2017.12.017.
[28] Tian, Z., Kale, V.S., Wang, Y., Kandambeth, S., Czaban-Jozwiak, J., Shekhah, O., Eddaoudi, M., Alshareef, H.N., 2021. High-capacity NH_4^+ charge storage in covalent organic frameworks. J Am Chem Soc 143, 19178–19186. https://doi.org/10.1021/jacs.1c09290.
[29] Tse Sum Bui, B., Mier, A., Haupt, K., 2023. Molecularly imprinted polymers as synthetic antibodies for protein recognition: the next generation. Small 19, e2206453. https://doi.org/10.1002/smll.202206453.
[30] Turiel, E., Martín-Esteban, A., 2019. Molecularly imprinted polymers-based microextraction techniques. Trends Anal Chem 118, 574–586. https://doi.org/10.1016/j.trac.2019.06.016.
[31] Wang, S., Shao, R., Li, W., Li, X., Sun, J., Jiao, S., Dai, S., Dou, M., Xu, R., Li, Q., Li, J., 2022. Three-dimensional ordered macroporous magnetic inverse photonic crystal microsphere-based molecularly imprinted polymer for selective capture of aflatoxin B1. ACS Appl Mater Interfaces 14, 18845–18853. https://doi.org/10.1021/acsami.2c01014.
[32] Wang, Y., Ma, X., Peng, Y., Liu, Y., Zhang, H., 2021. Selective and fast removal and determination of beta-lactam antibiotics in aqueous solution using multiple templates imprinted polymers based on magnetic hybrid carbon material. J Hazard Mater 416, 126098. https://doi.org/10.1016/j.jhazmat.2021.126098.
[33] Wang, Z., Zhang, S., Chen, Y., Zhang, Z., Ma, S., 2020. Covalent organic frameworks for separation applications. Chem Soc Rev 49, 708–735. https://doi.org/10.1039/c9cs00827f.
[34] Wei, L., Sun, T., Shi, Z., Xu, Z., Wen, W., Jiang, S., Zhao, Y., Ma, Y., Zhang, Y.B., 2022. Guest-adaptive molecular sensing in a dynamic 3D covalent organic framework. Nat Commun 13, 7936. https://doi.org/10.1038/s41467-022-35674-8.
[35] Xie, J., Jiang, H., Shen, J., Peng, T., Wang, J., Yao, K., Sun, S., Shao, B., Tang, J., 2017. Design of multifunctional nanostructure for ultrafast extraction and purification of aflatoxins in foodstuffs. Anal Chem 89, 10556–10564. https://doi.org/10.1021/acs.analchem.7b02777.
[36] Xu, H., Sun, J., Wang, H., Zhang, Y., Sun, X., 2021. Adsorption of aflatoxins and ochratoxins in edible vegetable oils with dopamine-coated magnetic multi-walled carbon nanotubes. Food Chem 365, 130409. https://doi.org/10.1016/j.foodchem.2021.130409.
[37] Xu, M., Zhou, L., Zhang, L., Zhang, S., Chen, F., Zhou, R., Hua, D., 2022. Two-dimensional imprinting strategy to create specific nanotrap for selective uranium adsorption with ultrahigh capacity. ACS Appl Mater Interfaces 14, 9408–9417. https://doi.org/10.1021/acsami.1c20543.
[38] Xu, M., Zhou, Z., Hao, L., Li, Z., Li, J., Wang, Q., Liu, W., Wang, C., Wang, Z., Wu, Q., 2023. Phenyl-imidazole based and nitrogen rich hyper-crosslinked polymer for sensitive determination of aflatoxins. Food Chem 405, 134847. https://doi.org/10.1016/j.foodchem.2022.134847.
[39] Yu, Z., Qiu, C., Huang, L., Gao, Y., Tang, D., 2023. Microelectromechanical microsystems-supported photothermal immunoassay for point-of-care testing of aflatoxin B1 in foodstuff. Anal Chem 95, 4212–4219. https://doi.org/10.1021/acs.analchem.2c05617.
[40] Yuan, X., Ferrer-Campos, R., Garces-Pineda, F.A., Villa, K., 2023. Molecular imprinted $BiVO_4$ microswimmers for selective target recognition and removal. Small 19, e2207303. https://doi.org/10.1002/smll.202207303.
[41] Yuan, Y., Yang, Y., Meihaus, K.R., Zhang, S., Ge, X., Zhang, W., Faller, R., Long, J. R., Zhu, G., 2023. Selective scandium ion capture through coordination templating in a covalent organic framework. Nat Chem. https://doi.org/10.1038/s41557-023-01273-3.
[42] Zhang, M., Li, Y., Yuan, W., Guo, X., Bai, C., Zou, Y., Long, H., Qi, Y., Li, S., Tao, G., Xia, C., Ma, L., 2021. Construction of flexible amine-linked covalent organic frameworks by catalysis and reduction of formic acid via the eschweiler-clarke reaction. Angew Chem Int Ed 60, 12396–12405. https://doi.org/10.1002/anie.202102373.
[43] Zhang, M., Zheng, R., Ma, Y., Chen, R., Sun, X., Sun, X., 2019. N-rich covalent organic frameworks with different pore size for high-pressure CO_2 adsorption. Micro Mesopor Mater 285, 70–79. https://doi.org/10.1016/j.micromeso.2019.04.021.
[44] Zhang, W., Chen, L., Dai, S., Zhao, C., Ma, C., Wei, L., Zhu, M., Chong, S.Y., Yang, H., Liu, L., Bai, Y., Yu, M., Xu, Y., Zhu, X.W., Zhu, Q., An, S., Sprick, R.S., Little, M.A., Wu, X., Jiang, S., Wu, Y., Zhang, Y.B., Tian, H., Zhu, W.H., Cooper, A. I., 2022. Reconstructed covalent organic frameworks. Nature 604, 72–79. https://doi.org/10.1038/s41586-022-04443-4.
[45] Zhang, X., Li, G., Wu, D., Zhang, B., Hu, N., Wang, H., Liu, J., Wu, Y., 2019. Recent advances in the construction of functionalized covalent organic frameworks and their applications to sensing. Biosens Bioelectron 145, 111699. https://doi.org/10.1016/j.bios.2019.111699.
[46] Zhang, Z., Kang, C., Peh, S.B., Shi, D., Yang, F., Liu, Q., Zhao, D., 2022. Efficient adsorption of acetylene over CO_2 in bioinspired covalent organic frameworks. J Am Chem Soc 144, 14992–14996. https://doi.org/10.1021/jacs.2c05309.
[47] Zhao, Q., Zhang, H., Zhao, H., Liu, J., Liu, J., Chen, Z., Li, B., Liao, X., Regenstein, J.M., Wang, J., Yang, X., 2020. Strategy of fusion covalent organic frameworks and molecularly imprinted polymers: a surprising effect in recognition and loading of cyanidin-3-o-glucoside. ACS Appl Mater Interfaces 12, 8751–8760. https://doi.org/10.1021/acsami.9b21460.
[48] Zhou, Z.B., Sun, H.H., Qi, Q.Y., Zhao, X., 2023. Gradually tuning the flexibility of two-dimensional covalent organic frameworks via stepwise structural transformation and their flexibility-dependent properties. Angew Chem Int Ed 62. https://doi.org/10.1002/anie.202305131.
[49] Zuo, J., Yan, T., Tang, X., Zhang, Q., Li, P., 2023. Dual-modal immunosensor made with the multifunction nanobody for fluorescent/colorimetric sensitive detection of aflatoxin B1 in maize. ACS Appl Mater Interfaces 15, 2771–2780. https://doi.org/10.1021/acsami.2c20269.